Hindawi
Geofluids
Volume 2023, Article ID 6930602, 10 pages
https://doi.org/10.1155/2023/6930602

Research Article

Integrated Geophysical and Geotechnical Approaches for Evaluating Dam Seepage in Lesser Himalayan Region of Pakistan

Umair Bin Nisar,[1] Muhammad Farooq,[2] Sarfraz Khan,[3] Ramesh Raj Pant,[4] Iftikhar A. Satti,[5] Ali Wahid,[2] Faizan ur Rehman Qaiser,[6] Syed Amjad Ali Bukhari,[6] and Furqan Mahmud Butt[1]

[1]*Department of Meteorology, COMSATS University Islamabad, Park Road, Tarlai Kalan, 45550 Islamabad, Pakistan*
[2]*Institute of Geology, University of Azad Jammu and Kashmir, Muzaffarabad, Azad Kashmir, Pakistan*
[3]*National Centre for Excellence in Geology, University of Peshawar, 25130 KP, Pakistan*
[4]*Central Department of Environmental Science, Tribhuvan University, Nepal*
[5]*Ayed Eid Al Osaimi Engineering Consulting Office, Al-Khobar, Saudi Arabia*
[6]*Department of Earth Sciences, COMSATS University Islamabad, Abbottabad Campus, Tobe Camp, Mandian, Abbottabad, KP, Pakistan*

Correspondence should be addressed to Ramesh Raj Pant; rpant@cdes.edu.np

Received 19 August 2022; Revised 11 January 2023; Accepted 12 January 2023; Published 28 February 2023

Academic Editor: Jianyong Han

Dam leakage is a major problem in earth-filled reservoir dams. The present research is aimed at detecting the seepage zones in an earth-filled reservoir dam in the vicinity of Sarobi village, North Waziristan, Pakistan. The objective was achieved by integrating geological, geotechnical, and geophysical datasets. Geological survey was carried out in the area to identify the surface exposures. Geotechnical data involved was used to estimation of permeability and Lugeon values to identify network of joints/fractures whereas electrical resistivity tomography (ERT) technique (utilizing Wenner-Schlumberger configuration) was applied for the identification of the leakage zones. Geological data revealed highly deformed alluvium towards the right abutment underlain by compressed shale and highly fractured limestone beds. Geotechnical data indicated high permeability, Lugeon values, and concentration of sand and gravel towards the right abutment whereas low permeability, Lugeon values, and higher concentration of silt and clay were observed towards the left abutment. ERT data identified a conductive zone embedded between impermeable lithologies having resistivity between 10 and 60 Ω·m. This conductive zone was observed in parallel profiles acquired in upstream, dam crest, and downstream parts of the dam. The integration of all the datasets revealed a network of joints that are interconnected and provide a path for water at the upstream side to pass through right abutment of dam and leak towards the downstream.

1. Introduction

Pakistan is a water-stressed country; it receives approximately 145 million-acre feet of water through precipitation and glacial melt, out of which it can only save 14 million-acre feet, wasting 131 million-acre feet to the sea [1, 2]. The loss is attributed to limited storage capacity/reservoirs [3]. In order to tackle the losses and support the irrigation requirement, the government of Pakistan has been focusing on achieving a "green revolution" by developing several small dams to support local agriculture [4, 5]. The majority of these small dams are earth-filled dams [6].

Earth-filled dams, among other types, are considered economical due to the composition of natural lithologies that are often available in the vicinity of the structure [7]. On the contrary, water leakage is a common problem in

earthen dams, and it usually occurs through either its foundations, the reservoir's bedrock, or the embankment-abutment contact. Tectonic, climate, and geological structures are the main factors that contribute to the occurrence of dam leakage processes [8, 9]. The leakage problem results in an increased discharge rate and ultimately affects the safety and stability of the dam structures. Several prominent disasters are associated with dam failures (i.e., immense property and environmental damages). Not long ago (in 1959), an earth-filled dam on the Machchu River in India collapsed, resulting in fatalities of approx. 18,000 people in downstream villages [10, 11]. In order to avoid such catastrophes, it is essential to develop a periodic monitoring system for leakage rates to prevent the collapse/failure of the dam.

Several techniques are used to track and monitor these leakages [12–17]. Conventional techniques involve hydrogeological investigations that are carried out through geological field visits and water level and temperature monitoring [18]. Geophysical methods, after their advent, have been widely used in detecting/monitoring different subsurface geological features [19]. Modern geophysical techniques such as ERT provide high-resolution images of the subsurface geological features [20, 21]. This technique has provided satisfactory results in characterizing the potential leakage pathways from earthen dams [8, 22–25]. These results help engineers provide appropriate technical solutions to minimize the rate of leakage, which is essential for the safety and stability of the dam [26–28].

The current study involves one of the similar dams that lie near the Sarobi village, North Waziristan (Figure 1). The Sarobi dam was constructed in 2018 in the proximity of Sarobi village on Ping Algad, which is 30 km southwest of Miranshah [29] (Figure 1). The catchment area of Ping Algad up to dam axis is 21 square km. The mean annual rainfall is about 330 mm, and the mean annual inflow is estimated at 1035 acre-ft [30]. This earth-filled dam has a clay and silt core and is 134 m long and 31 m high with a 10 m wide crest. The dam has a maximum reservoir capacity of 1250 acre-ft. In 2018, the average water drop in the dam reservoir was 30 cm per day. Hydrogeological perspective reveals Jurassic to Cretaceous Limestone Formation as the main groundwater aquifer in the area. The aquifer is characterized by high groundwater permeability due to fracturing occurs at variable depths. The tube wells drilled in the limestone produced ample amounts of groundwater for domestic usage [31]. Generally, in this region, the direction of surface water and groundwater flow is from northwest to southeast direction. The aquifer is recharged from precipitation and perennial streams from the surrounding hilltops [31].

The present research focuses on integrating geological, geotechnical, and geophysical approaches to resolve the hydrogeological problems associated with dam leakages in the study area. The geophysical data in relation to geological and geotechnical datasets were utilized to identify the leakages, with their patterns and extent. The study will be helpful for the engineers to plan the remedial measures and address similar issues with other earthen dams.

2. Material and Methods

2.1. Surface and Subsurface Geological Data. The geological field observations were carried out while surveying the area. All the necessary photographs showing variations in surficial features were taken. Structural features such as faults, joints, fracture, and shearing were noted during the survey (Figure 2). To identify the subsurface lithologies and to gather information regarding the physical properties of the rocks (surrounding the dam wall), six boreholes, having variable depths, were drilled at different locations along the dam axis (Table 1). The boreholes are located at the base of dam axis in Nullah bed (borehole 1), at the right abutment of the saddle (borehole 2), in exposed bedrock at the left abutment (borehole 3), at the right abutment (borehole 4), and into exposed bedrock (boreholes 5 and 6). The depth of boreholes varies from 10 m to 25 m (Table 1).

2.2. Electrical Resistivity Data Acquisition. Electrical Resistivity Tomography (ERT) has been used extensively for hydrogeological, engineering, and environmental issues [21, 32]. The ERT measurements were performed using Geomative GD-10. The instrument is equipped with a switching box, intelligent cable, and electrodes.

Sixty electrodes were installed in a straight line along the measured profile. Wenner-Schlumberger configuration was adopted to achieve depth and lateral coverage [19]. The interval between electrodes was kept at 5 m in all the acquired profiles. The total number of data levels was 29. All the profiles had a uniform length of 300 m and a depth of up to 50-60 m. Out of three (03) acquired profiles, two (02) profiles were acquired along the up- and downstream at distances of 5 m and 50 m away from the dam, respectively, whereas profile 2 (Figure 1) was acquired at the topside of the dam axis. All three profiles were oriented north-south.

The acquired ERT dataset was processed using RES2DINV software developed by Loke and Barker [33]. The least-squares method with smoothing of model resistivity was adopted for obtaining better results. The optimization of this technique fundamentally depends on minimizing the difference between measured and calculated apparent resistivity values, and the difference is articulated in the form of root mean square error (RMSE). The software provides noisy point adjustments before running the inversion to avoid high RMSE ranging from 09% to 3.5%. The resistivity method's resolution decreases exponentially with depth, and factor is typically adjusted to achieve stabilization in the inversion method as the layer becomes deeper. In the current study, the factor was raised by 1.05 times to achieve stabilization. The inverted resistivity values were then classified into different lithological units based on the available geological and borehole data (Table 2).

2.3. Geotechnical Data Acquisition. The rock sample and core data from 5 test pits drilled at different locations (Figure 1) around the dam were used to assess geotechnical parameters. The water pressure tests (Table 3) were carried out, and Lugeon values [34] were obtained, providing

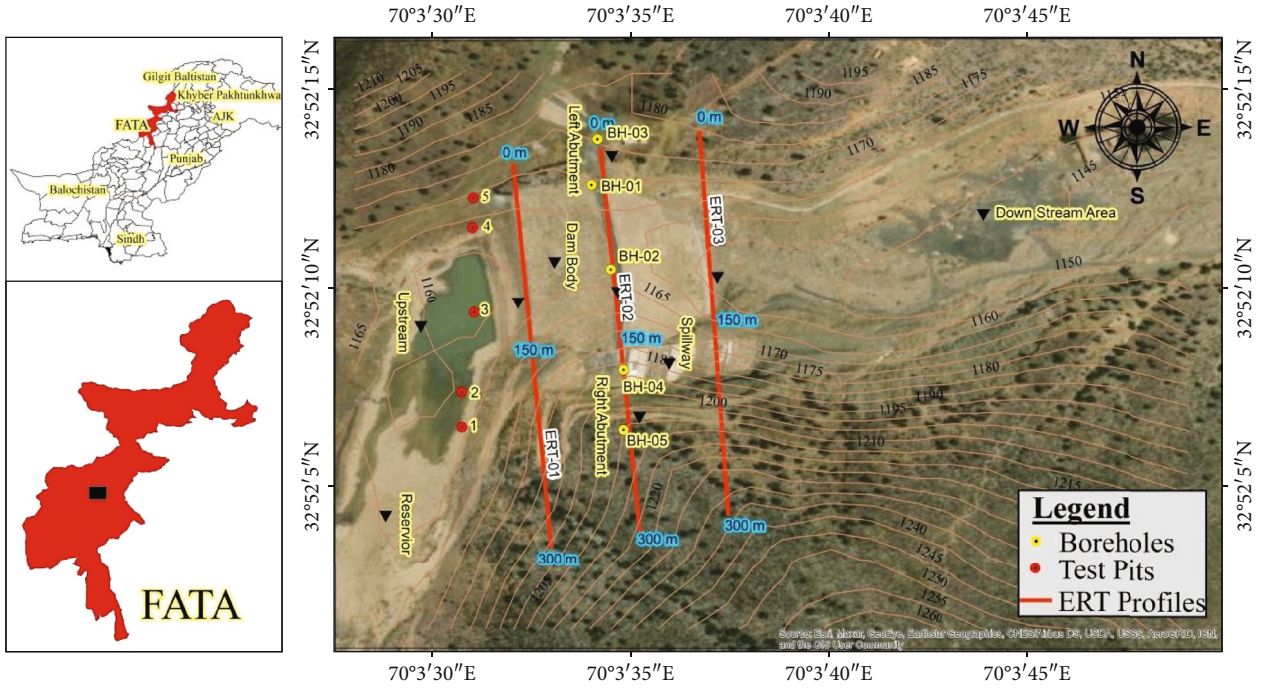

Figure 1: Map of the study area showing location of boreholes, ERT profiles, and test pits.

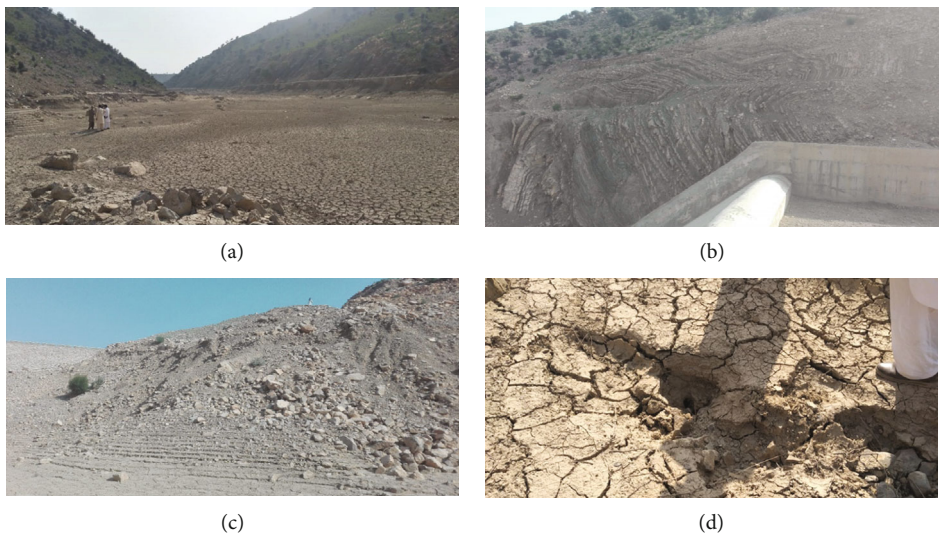

Figure 2: (a) Showing fluvial deposits, (b) showing crushed material towards right abutment, (c) alluvium towards the right abutment and water marks due to lowering of reservoir, and (d) mud cracks.

information about the fractures and joints in the lithologies encountered [35]. The geotechnical tests (Table 4) included bulk density, grain size analysis, Atterberg limits, Proctor test, and direct shear test [36, 37]. The standard ASTM sieve openings considered for grain size analysis were 4.75-75 mm (gravel), 0.075-4.75 mm (sand), 0.002-0.075 mm (silt), and <0.002 mm (clay). The core recovery also provided information about compact and loose lithologies [38, 39]. Rock Quality Designation (RQD) values [40] also demarcated the joints and fracture information that were correlated with available results of ERT and surface geology [39, 41–43].

3. Results and Discussion

3.1. Geological Data. The surface geology of the dam's reservoir area comprises mainly of Quaternary deposits, such as clays, sands, gravels, and boulders as shallow materials (Figure 2). The thickness of these deposits varies up to one meter. These alluvial deposits overlay the Jurassic to Cretaceous limestone with interbedded shale (Kurram Group) that comprises the bedrock of the dam's reservoir [44]. Kurram Group rocks are dipping towards the upstream at an angle of 35-45 degrees; extensive fracturing and

Table 1: Depth and locations of the boreholes.

Sr. no.	Borehole no.	Location	Depth (m)
1	1	Nullah bed Dam axis	20
2	2	Right abutment of saddle	20
3	3	Left abutment	25
4	4	Right abutment	13
5	5	Spillway right abutment	10
6	6	Spillway *d*/*t* dam axis	10

Table 2: Resistivity values assigned to different lithologies [19].

Sr no.	Resistivity (Ω·m)	Lithology
1	≤25	Saturated clays/silts
2	25-80	Saturated highly fractured limestone
3	80-500	Moderately fractured limestone
4	500-3000	Compacted limestone with interbedded shale

karstification have been observed during the field investigation (Figure 2). The spillway of the dam is located on the right bank, and its upstream side has complexed geology (Figure 3). When the dam reservoir's water level is decreased, mud cracks were developed (Figure 2).

The overall structural geometry of the rock is dipping at the upstream side of the dam; however, due to the overturning of folded and thrust fault systems, the right abutment rock dips toward the downstream side (Figure 3). Therefore, the rock joints and fractures have similar trend to reservoir's water flow direction [45].

Six boreholes drilled in the vicinity of the dams' revealed useful information that further strengthened the surface geological arguments. Borehole 1, drilled in the Nullah bed upstream of the dam axis, revealed the thickest sediment cover, comprising clay. The overburden was underlain by alternating beds of limestone and shale (Figure 3). Borehole 2 revealed thin sediment cover (up to 5 m) comprising limestone and interbedded shale.

The presence of a surficial clay cover serves as a blanket to further prevent seepage [46]. Borehole 3 revealed no surficial overburden due the exposure of the bedrock at the surface. The observed bedrock was fractured and jointed, with alternating beds of shale (Figure 3). Boreholes 4, 5, and 6 revealed near surface fractured/jointed limestone and alternating layers of shale (Figure 3). Further geotechnical investigations also suggested the poor quality of the rock encountered in these wells as compared to the first three boreholes with good protective clay cover. The presence of open joints near the studied boreholes is in the direction of the seepage of water flow (Figure 2).

3.2. Electrical Resistivity Tomography (ERT). The inverted ERT model shows the subsurface resistivity values of the geological formations beneath the dam's reservoir area [15]. The obtained results were derived from 2D inversion and were interpreted based on geological field observation and geotechnical data [47, 48].

3.2.1. ERT-1 (Upstream). Figure 4 represents the inverted resistivity section of the ERT-1 profile. The profile is acquired in the upstream area having a length of 300 m. Clay, sands, and gravel, covering the shallow parts with moderate resistivity values (200-500 $\Omega \cdot m$) of ERT-1. The alluvium appears to be irregular in thickness because of the irregularity of the eroded surface (Figure 4). The starting section of the ERT-1 profile shows low resistivity (100-200 Ω·m) from the beginning to a horizontal distance of 80 m, comprising of fractured limestone, and is partly saturated (Figure 4). This decreases the overall electrical resistivity values of the upper zone [32]. The middle section of the profile (100 m to 150 m) comprises partly fractured 10 to 30 m thick bedrock (200-500 $\Omega \cdot m$). This section is followed by a highly fractured carbonate rock (limestone) filled with dam reservoir's water seepage as indicated by low resistivity (10 to 60 Ω·m) (Figure 4). This low resistive zone is developed due to percolation of base flow beneath the main dam body [22, 32]. In Figure 4, the clear image of the approximately 10 m excavated zone at a distance of 160 m of the spillway is shown.

The upper portion of the end section of ERT-1 from 175 to 210 m comprises partly fractured limestone with moderate electrical resistivity values (100-250 Ω·m). Nevertheless, the lower portion on the right side profile shows an anomalous zone (Figure 4) having resistive values of <60 Ω·m. This anomalous feature is similar to ERT-3, which clearly indicates the linear correlation between upstream and downstream images (Figures 4 and 5). During the 2018 flash flood, seepage water was oozing on the right abutment side [29]. Hence, the correlation suggests that both the joints' sets are interconnected and cause the dam reservoir to leak [17].

3.2.2. ERT-2 (Dam Crest). ERT-2 was acquired on the dam crest; having a spread length of 300 m. Figure 6 depicts an inverted cross-section of the ERT-2 profile. Half of the electrodes were installed on the dam crest, and the remaining was installed on the natural ground, hence resulting in an undulating topography (Figure 1). The main dam body is extending to a depth of 35 m, represented by ERT-2 profile, and is comprised of clay and silty material (Figures 3 and 6). The lower part of the core comprises coarser materials as indicated by resistivity values of <30 to ~60 Ω·m. However, the upper part composes of mostly clayey material (Figure 6) that is often saturated as resistivity values ranges below 20 Ω·m due to less permeability [14].

Surface geological conditions on the right abutment show a highly deformed zone indicating tectonic activities in the past (Figure 2). The southern right part of the ERT-2 below 160-300 m represents the deformed zone (Figure 6). This zone indicated high resistivity values (500-2500 Ω·m), especially near the surface. An interesting anomaly having low resistivity values (≥60 Ω·m) was found embedded within high resistivity values (Figure 6). This anomaly is attributed to fractures filled with dam seepage water [14].

Table 3: Results of geotechnical study.

Test pit no.	Depth (m)	Bulk density (mg/m^3)	Grain size analysis				Atterberg limits			Proctor test		Direct shear test		Permeability (cm/s)
			Gravel (%)	Sand (%)	Silt (%)	Clay (%)	LL (%)	PI (%)	PL (%)	OMC (%)	MDD (mg/m^3)	C (K Pa)	Phi (degrees)	
TP-1	7.0-8.0	2.025	70	30										
TP-2	3.0-4.0	2.025	97	3										
TP-3	5.0-6.0		23		39	38	28	16	12	14.5	1.835	4	24	5.24×10^{-7}
TP-4	3.0-4.0		23		45	32	27	16	11	14.2	1.883	7	26	3.88×10^{-7}
TP-4	5.0-6.0													
TP-5	3.0-4.0		23		40	37	30	18	12	12.3	1.86	5	27	4.75×10^{-7}

Table 4: Results of water tests carried out at different bores.

Borehole no.	Depth (m)	Flow rate (liters/min)	Lugeon value (L)	Rock type
4	3	60	56	Limestone and shale
4	6	68	29.6	
4	10	55	26.8	
5	2	58	Nil	
5	5	45	Nil	
5	8	42	Nil	
6	2	58	44	
6	5	36	Nil	

3.2.3. ERT-3 (Downstream). The starting section (north) of the ERT-3 profile from the beginning to a horizontal distance of 80 m is composed of fractured limestone. It is partly saturated decreasing the overall electrical resistivity values of upper zone [22, 32, 49, 50] (Figure 5). The lower section (similar to ERT-1) is attributed to joint set at the left side of the dam abutment and facilitate in percolation of base groundwater flow passing beneath the main dam body. The middle section (100 to150 m) comprised of partly fractured 10 to 30 m thick bedrock (10-20 Ω·m) having resistivity of 10-20 Ω·m. This section is followed by low resistivity (10-60 Ω·m) highly fractured carbonate rock filled with dam reservoir's seepage water (Figure 5). The excavated zone (10 m depth) of the spillway is clearly visible in Figure 5. The presence of very compact bedrock below spillway revealed about a barrier for any seepage.

The ending section (south) of ERT-3 profile from 175 to 210 m is composed of partly fractured limestone (500-1500 Ω·m) at the upper portion. Similar to ERT-1 and ERT-2, the lower portion (south of ERT-3) reveals an anomalous zone of low resistivity values $< 60\,\Omega \cdot \mathrm{m}$ compared to surrounding strata that indicates a linear correlation between upstream and downstream anomalies (Figures 4 and 6).

The all three ERT profiles provided a generalized behavior of geological units beneath and in the vicinity of the Sarobi dam structure. These profiles revealed a conductive zone towards the right abutment (in south) (Figures 4–6). This conductive zone was also identified in upstream and downstream profiles as a low resistivity saturated zone embedded between high resistivity lithology (Figures 4–6). This zone represents set of interconnected joints that starts from upstream profile. While passing through the loosely pack alluvium, it bypasses the dam and reaches the downstream part [22]. These interconnected joints network serve as a leakage path way from up to downstream while passing near the right abutment [13]. The left abutment due to presence of clays (Figure 6) serves as a barrier for any seepage from left side of dam. Martínez-Moreno et al. [16] carried out similar ERT and IP studies to detect subsurface leakage zones. In his study, conductive zones were demarcated within high resistivity zones that were transmitting the leakage water. Lin et al. [15] carried out ERT profiles on upstream dam crest and downstream shell to detect the abnormal seepage in earth dam (classified low resistivity water intake zones causing seepage) in Taiwan. The advancement in the study of Lin et al. [15] were carrying out time-lapse data to monitor, which is recommended in our study as well.

3.3. Geotechnical Characteristics of Sarobi Dam. The geotechnical characteristics of Sarobi dam were evaluated using five dug pits of variable depth (Table 3). Dug pits 1 and 2 represent permeable coarser lithologies of gravel and sand. These lithologies will create large pore water pressure in the soils which will temporarily decrease the shear strength [51].

Dug pits 3, 4, and 5 comprise a mix ratio of gravel, silt, and clay (Table 3). The concentration of clay and silt increases while moving from the right to the left abutment (Figure 6). The coefficient of permeability of pit 3 (5.24×10^{-7}) and 4 (3.88×10^{-7}) indicates that the material is less permeable resulted in slow drain water through the soil. Furthermore, there is a decrease in permeability values from the right to the left abutment, indicting presence of finer lithologies that tends to protect the dam from further leakage [12]. Similar results were revealed by ERT datasets which increases the reliability of geotechnical results (Figures 2 and 6).

3.4. Integration of Electrical Resistivity Tomography, Borehole, and Geotechnical Data. The integration of the results of geological, electrical resistivity, and geotechnical investigations was done to identify the true subsurface conditions. The surficial geology revealed the presence of alluvium cover (at upstream and right abutment side) followed by gentle dipping fractured limestone, interbedded with shale, at a depth of 1 to ~3 meter (Figure 2) which is confirmed from the boreholes (Table 1).

The geotechnical results revealed the presence of poor quality rock based on Rock Quality Designation (RQD) (0 to ~10%) and core recovery (15 to ~50%) values. The results of water pressure test (26-60 Lugeon values) at the upstream and right abutment side (Table 3) indicate the presence of open joints in subsurface [52]. These joints were also identified in ERT profiles 1, 2, and 3 (Figures 4–6) by low resistivity values of <60 Ω·m towards the upstream, the right abutment, and downstream [53]. This low resistivity zone is (embedded between the lithologies with high resistivity values) often indicated by the geological and geotechnical parameters that is attributed to the leakage from highly fractured and loose lithology [54].

Likewise, moderate dip rock of moderately weathered, folded, and fractured limestone interbedded with shale is exposed at surface of the left abutment of dam (Figures 2, 3, and 6). Same lithology is resulted in the borehole 3 at the left abutment (drilled up to 25 m). The limestone was encountered up to 17 m followed by alternate layer of interbedded shale up to 25 m. From the geotechnical investigations, 23-70% rock is recovered with variation in Rock Quality Designation values of 0-39% and Lugeon water pressure value of 62.7 (for upper 5 m). This value decreases as the borehole depth increases (Tables 3 and 4). The resistivity

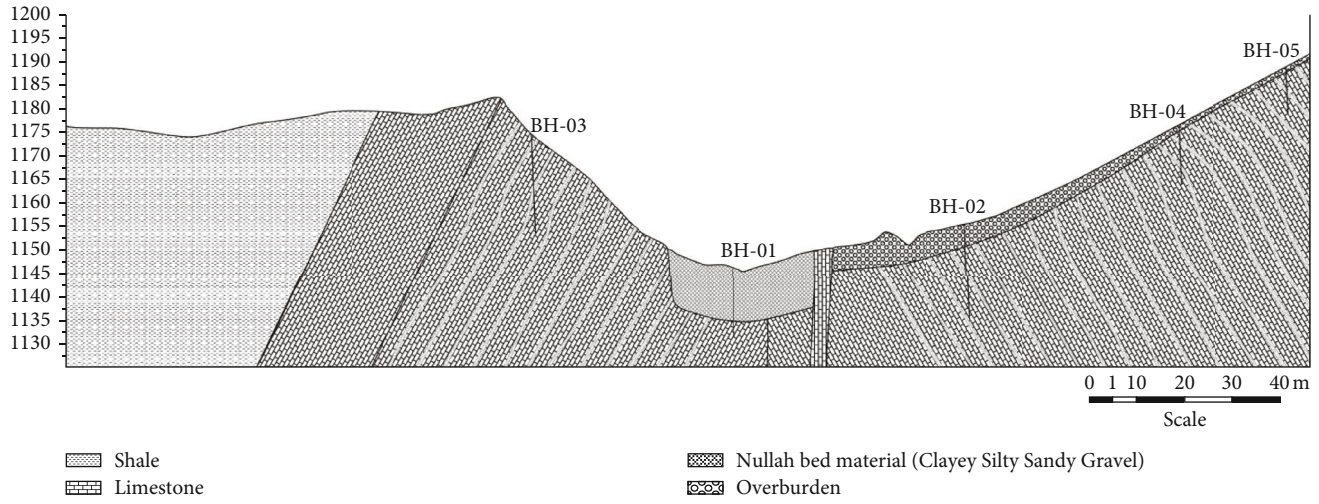

Figure 3: Geological cross-section of the dam indicating positions of the boreholes and lithological pattern.

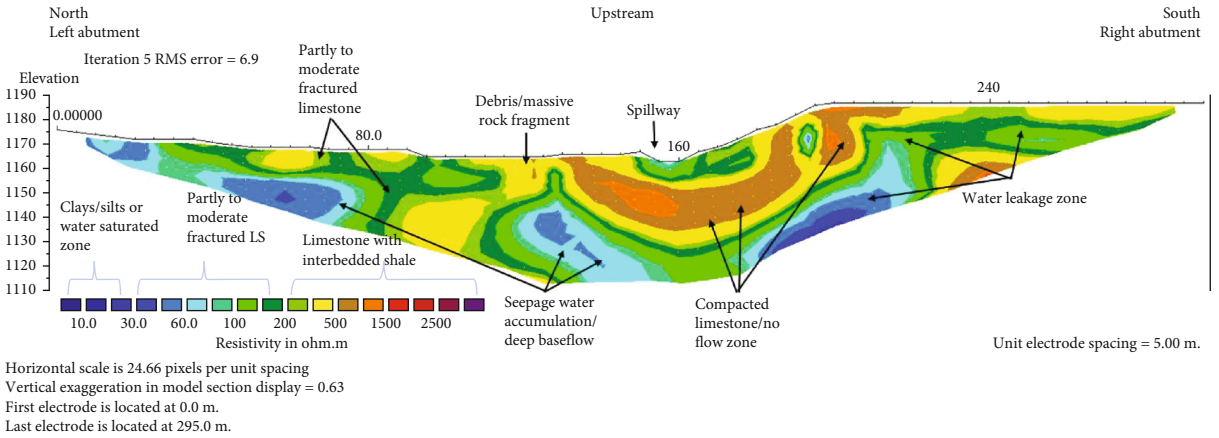

Figure 4: ERT-1 acquired upstream of the Sarobi Dam.

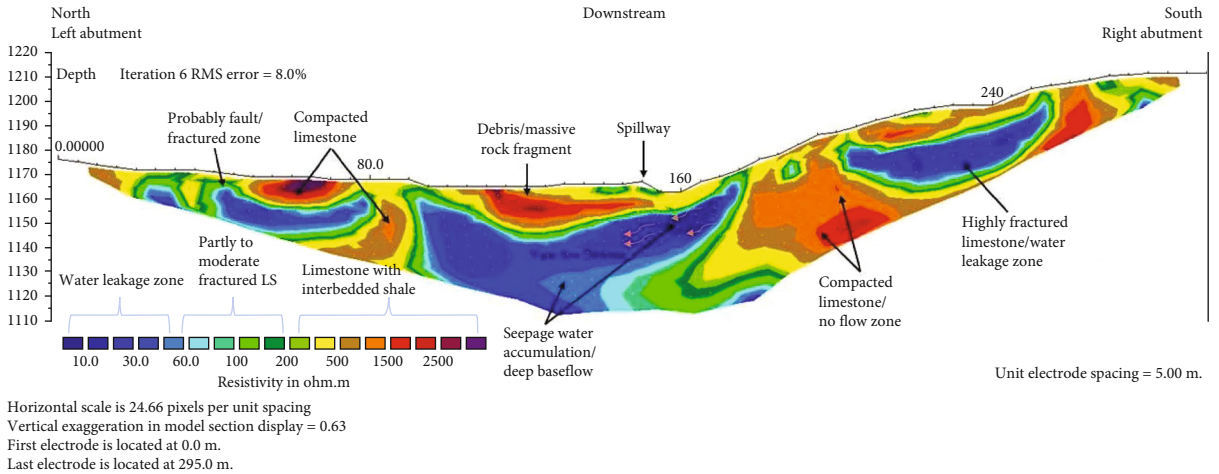

Figure 5: ERT acquired downstream of the Sarobi Dam.

values (at the left abutment) also indicated high values towards the upstream (profile 1) and downstream (profile 3) of the dam (Figures 4–6), these high values were attributed to compacted limestone interbedded with shale [55]. However, the dam axis (profile 2) indicated low values (Figures 3 and 6) that were attributed to the presence of

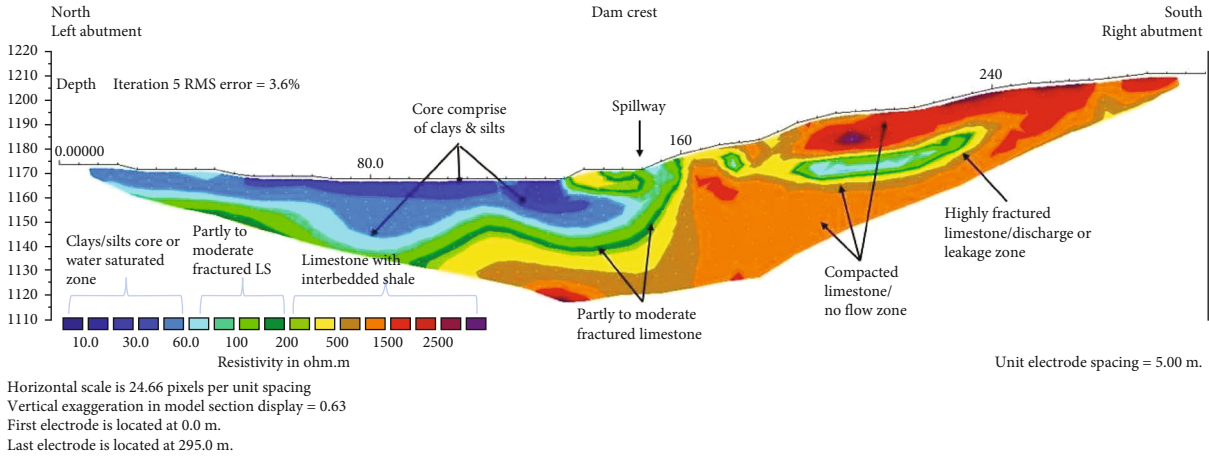

Figure 6: ERT acquired on crest of the Sarobi Dam.

saturated shale/clays that tend to decrease the resistivity values but do not support the leakage [53].

4. Conclusions

The integration of geological, geophysical, and geotechnical datasets has yielded significant results in demarcation of seepage zones. The borehole data in accordance with the surface geological data revealed exposure of highly weathered silt, clay as overlying lithologies (with thickness up to 5 m) on alternating beds of fractured limestone and shale. Furthermore, these datasets identified joints in the limestone beds towards the right abutment that are interconnected.

The ERT sections identified a very clear low resistivity zone (10-60 Ω·m) towards the upstream, right abutment, and downstream areas of the dam. This zone has thickness from 08 m to 20mmostly lying within lateral distance of 160 to 240 m. These low values indicate network of interconnected joints (seepage zones) towards the right abutment.

The high Lugeon values mostly fall between 26 and 60 and indicate open joints in subsurface. The Atterberg test in close accordance with the geological and ERT data also verified concentrations of silt and saturated clay towards the center and left of the dam abutment. But these lithologies are not permeable resulting in prevention of any leakage from the left abutment. The integration of all the datasets revealed a highly fractured and connected zone starting from upstream area passing through the right abutment and reaching the downstream side of the dam. The storage water leaks through this connected zone.

It is recommended to carryout time-lapse ERT modeling along with the boreholes (having more depth) coupled with piezometric information of water wells to identify possible water level changes due to dam leakage.

Data Availability

The data used to support the findings of this study were supplied by Dr. Umair Bin Nisar under license and so cannot be made freely available. Requests for access to these data should be made to Dr. Umair Bin Nisar (umair.nisar@comsats.edu.pk).

Conflicts of Interest

The authors declare that they have no conflicts of interest.

Acknowledgments

The authors thank the Institute of Geology, University of Azad Jammu and Kashmir, for providing field equipment and funding for the current research work.

References

[1] S. Riaz, W. Ishaque, and M. A. Baig, "Indian aqua aggression: investigating the impact of Indus Water Treaty (Iwt) on future of India-Pakistan water dispute," *NDU Journal*, vol. 34, pp. 131–146, 2020.

[2] S. Meer, "Dw News, water crisis: why is Pakistan running dry?," 2018, https://www.dw.com/en/water-crisis-why-is-pakistan-running-dry/a-44110280.

[3] "The News," 2020, https://www.thenews.com.pk/print/755861-saving%20water?__cf_chl_managed_tk__=bd2YE2M7WnzpZZfJMott6s_Gc0d8llaUUNcnPid9S9A-1641452013-0-gaNycGzNC_0)%20.

[4] I. Ahmad, S. A. H. Shah, and M. S. Zahid, "Why the Green Revolution was short run phenomena in the development process of Pakistan: a lesson for future," *Journal of Rural Development & Administration*, vol. 4, no. 35, pp. 89–104, 2004.

[5] M. Ashraf, M. A. Kahlown, and A. Ashfaq, "Impact of small dams on agriculture and groundwater development: a case study from Pakistan," *Agricultural Water Management*, vol. 92, no. 1-2, pp. 90–98, 2007.

[6] A. Wajid, A. Usman, M. K. Khan, and A. A. Chaudhry, "Socio economic impact of small dams on local vicinity: a case study of Aza Khel Dam Peshawar," *Global Journal of Management and Business Research Economics and Commerce*, vol. 13, no. 5, pp. 30–39, 2013.

[7] V. Singh, *Dam Breach Modeling Technology, (Vol. 17)*, Springer Science & Business Media, 1996.

[8] W. Al-Fares, "Application of electrical resistivity tomography technique for characterizing leakage problem in Abu Baara Earth Dam, Syria," *International Journal of Geophysics*, vol. 2014, Article ID 368128, 9 pages, 2014.

[9] P. A. Bedrosian, B. L. Burton, M. H. Powers, B. J. Minsley, J. D. Phillips, and L. E. Hunter, "Geophysical investigations of geology and structure at the Martis Creek Dam, Truckee, California," *Journal of Applied Geophysics*, vol. 77, pp. 7–20, 2012.

[10] S. B. Easwaran, *The Loudest Crash of '79*, Outlook India, 2012.

[11] World Bank Environment Dept, *Environmental Assessment Sourcebook*, World Bank Publications, 1991.

[12] N. Adamo, N. Al-Ansari, V. Sissakian, J. Laue, and S. Knutsson, "Geophysical methods and their applications in dam safety monitoring," *Journal of Earth Sciences and Geotechnical Engineering*, vol. 11, no. 1, pp. 291–345, 2021.

[13] R. Adinehvand, E. Raeisi, and A. Hartmann, "An integrated hydrogeological approach to evaluate the leakage potential from a complex and fractured karst aquifer, example of Abolabbas Dam (Iran)," *Environmental Earth Sciences*, vol. 79, no. 22, article 501, 2020.

[14] D. A. Gunn, J. E. Chambers, B. E. Dashwood et al., "Deterioration model and condition monitoring of aged railway embankment using non-invasive geophysics," *Construction and Building Materials*, vol. 170, pp. 668–678, 2018.

[15] C. P. Lin, Y. C. Hung, Z. H. Yu, and P. L. Wu, "Investigation of abnormal seepages in an earth dam using resistivity tomography," *Journal of GeoEngineering*, vol. 8, no. 2, pp. 61–70, 2013.

[16] F. J. Martínez-Moreno, F. Delgado-Ramos, J. Galindo-Zaldívar, W. Martín-Rosales, M. López-Chicano, and L. González-Castillo, "Identification of leakage and potential areas for internal erosion combining ERT and IP techniques at the Negratin Dam left abutment (Granada, southern Spain)," *Engineering Geology*, vol. 240, pp. 74–80, 2018.

[17] J. D. Rice and J. M. Duncan, "Findings of case histories on the long-term performance of seepage barriers in dams," *Journal of Geotechnical and Geoenvironmental Engineering*, vol. 136, no. 1, pp. 2–15, 2010.

[18] G. Berhane, K. Martens, N. Al Farrah, and K. Walraevens, "Water leakage investigation of micro-dam reservoirs in Mesozoic sedimentary sequences in Northern Ethiopia," *Journal of African Earth Sciences*, vol. 79, pp. 98–110, 2013.

[19] U. B. Nisar, M. J. Khan, M. Imran et al., "Groundwater investigations in the Hattar industrial estate and its vicinity, Haripur district, Pakistan: an integrated approach," *Kuwait Journal of Science*, vol. 48, no. 1, pp. 51–61, 2021.

[20] A. Aina, M. O. Olorunfemi, and J. S. Ojo, "An integration of aeromagnetic and electrical resistivity methods in dam site investigation," *Bulletin of the International Association of Engineering Geology*, vol. 51, no. 1, pp. 31–38, 1995.

[21] S. C. H. Lee, K. A. M. Noh, and M. N. A. Zakariah, "High-resolution electrical resistivity tomography and seismic refraction for groundwater exploration in fracture hard rocks: a case study in Kanthan, Perak, Malaysia," *Journal of Asian Earth Sciences*, vol. 218, article 104880, 2021.

[22] W. Al-Fares, "Contribution of the geophysical methods in characterizing the water leakage in Afamia B Dam, Syria," *Journal of Applied Geophysics*, vol. 75, no. 3, pp. 464–471, 2011.

[23] A. D. Chinedu and A. J. Ogah, "Electrical resistivity imaging of suspected seepage channels in an earthen dam in Zaria, Northwestern Nigeria," *Open Journal of Applied Sciences*, vol. 3, no. 1, pp. 145–154, 2013.

[24] I. K. Cho and J. Y. Yeom, "Crossline resistivity tomography for the delineation of anomalous seepage pathways in an embankment dam," *Geophysics*, vol. 72, no. 2, pp. G31–G38, 2007.

[25] S. Thompson, B. Kulessa, and A. Luckman, "Integrated electrical resistivity tomography (ERT) and self-potential (SP) techniques for assessing hydrological processes within glacial lake moraine dams," *Journal of Glaciology*, vol. 58, no. 211, pp. 849–858, 2012.

[26] M. R. Boroomand and A. Mohammadi, "Evaluation of earth dam leakage considering the uncertainty in soil hydraulic parameters," *Civil Engineering Journal*, vol. 5, no. 7, pp. 1543–1556, 2019.

[27] F. Gutiérrez, M. Mozafari, D. Carbonel, R. Gómez, and E. Raeisi, "Leakage problems in dams built on evaporites. The case of La Loteta Dam (NE Spain), a reservoir in a large karstic depression generated by interstratal salt dissolution," *Engineering Geology*, vol. 185, pp. 139–154, 2015.

[28] S. J. Ikard, A. Revil, M. Schmutz, M. Karaoulis, A. Jardani, and M. Mooney, "Characterization of focused seepage through an earthfill dam using geoelectrical methods," *Groundwater*, vol. 52, no. 6, pp. 952–965, 2014.

[29] K. Wisal, K. Asif, K. A. Ullah, and K. Mujahid, "Evaluation of hydrological modeling using climatic station and gridded precipitation dataset," *Mausam*, vol. 71, no. 4, pp. 717–728, 2020.

[30] M. Nafees, A. Shabir, and U. Zahid, "Construction of dam on Kabul River and its socio-economic implication for Khyber Pukhtunkhwa, Pakistan," in *Seminar on Pak–Afghan Water Sharing*, SASSI, Springville, IN, USA, 2016.

[31] Y. M. Taraky, E. McBean, Y. Liu et al., "The role of large dams in a transboundary drought management co-operation framework-case study of the Kabul River Basin," *Water*, vol. 13, no. 19, article 2628, 2021.

[32] D. F. Rucker, C. H. Tsai, K. C. Carroll et al., "Bedrock architecture, soil texture, and hyporheic zone characterization combining electrical resistivity and induced polarization imaging," *Journal of Applied Geophysics*, vol. 188, article 104306, 2021.

[33] M. H. Loke and R. D. Barker, "Practical techniques for 3D resistivity surveys and data inversion1," *Geophysical Prospecting*, vol. 44, no. 3, pp. 499–523, 1996.

[34] M. Ghafoori, G. R. Lashkaripour, and S. Tarigh Azali, "Investigation of the geological and geotechnical characteristics of Daroongar Dam, Northeast Iran," *Geotechnical and Geological Engineering*, vol. 29, no. 6, pp. 961–975, 2011.

[35] D. Akbarimehr and E. Aflaki, "Site investigation and use of artificial neural networks to predict rock permeability at the Siazakh Dam, Iran," *Quarterly Journal of Engineering Geology and Hydrogeology*, vol. 52, no. 2, pp. 230–239, 2019.

[36] M. A. Dafalla, "Effects of clay and moisture content on direct shear tests for clay-sand mixtures," *Advances in Materials Science and Engineering*, vol. 2013, Article ID 562726, 8 pages, 2013.

[37] O. Igwe and J. C. Egbueri, "The characteristics and the erodibility potentials of soils from different geologic formations in Anambra State, Southeastern Nigeria," *Journal of the Geological Society of India*, vol. 92, no. 4, pp. 471–478, 2018.

[38] A. Azimian and R. Ajalloeian, "Comparison between Lugeon with secondary permeability index obtained of water pressure test in rock masses," *Electronic Journal of Geotechnical Engineering*, vol. 18, pp. 1603–1612, 2013.

[39] Q. Zhang and Z. Wang, "Spatial prediction of loose aquifer water abundance mapping based on a hybrid statistical learning approach," *Earth Science Informatics*, vol. 14, no. 3, pp. 1349–1365, 2021.

[40] D. Deere and D. W. Deere, "The Rock Quality Designation (RQD) index in practice," in *Rock classification systems for engineering purposes*, ASTM International, 1988.

[41] A. S. Akingboye and A. A. Bery, "Characteristics and rippability conditions of near-surface lithologic units (Penang Island, Malaysia) derived from multimethod geotomographic models and geostatistics," *Journal of Applied Geophysics*, vol. 204, article 104723, 2022.

[42] M. Hasan, Y. Shang, H. Meng, P. Shao, and X. Yi, "Application of electrical resistivity tomography (ERT) for rock mass quality evaluation," *Scientific Reports*, vol. 11, no. 1, article 23683, 2021.

[43] M. Hasan, Y. Shang, P. Shao, X. Yi, and H. Meng, "Geophysical research on rock mass quality evaluation for infrastructure design," *Earth and Space Science*, vol. 9, no. 1, 2022.

[44] M. A. Khan, I. A. Abbasi, A. W. Qureshi, and S. R. Khan, "Tectonics of Afghan-India collision zone, Kurram-Waziristan region," in *Conference Proceedings of the Annual Technical Conference*, pp. 219–234, Pakistan, 2003.

[45] E. Asadollahpour, A. Baghbanan, H. Hashemolhosseini, and E. Mohtarami, "The etching and hydraulic conductivity of acidized rough fractures," *Journal of Petroleum Science and Engineering*, vol. 166, pp. 704–717, 2018.

[46] B. W. Buck and R. J. Bayer, "Geologic and hydrologic considerations for construction of cyanide heap leach facilities," in *Proceedings Symposium on Geology and Hydrology of Hazardous-Waste, Mining-Waste, Waste-Water and Repositories Sites in Utah, Salt Lake City*, Salt Lake City, 1989.

[47] T. R. Andersen, S. E. Poulsen, M. A. Pagola, and A. B. Medhus, "Geophysical mapping and 3D geological modelling to support urban planning: a case study from Vejle, Denmark," *Journal of Applied Geophysics*, vol. 180, article 104130, 2020.

[48] M. M. Crawford, L. S. Bryson, E. W. Woolery, and Z. Wang, "Using 2-D electrical resistivity imaging for joint geophysical and geotechnical characterization of shallow landslides," *Journal of Applied Geophysics*, vol. 157, pp. 37–46, 2018.

[49] J. A. M. González, J. C. Comte, A. Legchenko, U. Ofterdinger, and D. Healy, "Quantification of groundwater storage heterogeneity in weathered/fractured basement rock aquifers using electrical resistivity tomography: sensitivity and uncertainty associated with petrophysical modelling," *Journal of Hydrology*, vol. 593, article 125637, 2021.

[50] C. R. Murphy, N. J. Finnegan, and F. K. J. Oberle, "Vadose zone thickness limits pore-fluid pressure rise in a large, slow-moving earthflow," *Journal of Geophysical Research: Earth Surface*, vol. 127, no. 6, 2022.

[51] Y. L. Chen, G. Y. Liu, N. Li, X. Du, S. R. Wang, and R. Azzam, "Stability evaluation of slope subjected to seismic effect combined with consequent rainfall," *Engineering Geology*, vol. 266, article 105461, 2020.

[52] J. E. Chambers, O. Kuras, P. I. Meldrum, R. D. Ogilvy, and J. Hollands, "Electrical resistivity tomography applied to geologic, hydrogeologic, and engineering investigations at a former waste-disposal site," *Geophysics*, vol. 71, no. 6, pp. B231–B239, 2006.

[53] T. Kalscheuer, M. Bastani, S. Donohue et al., "Delineation of a quick clay zone at Smørgrav, Norway, with electromagnetic methods under geotechnical constraints," *Journal of Applied Geophysics*, vol. 92, pp. 121–136, 2013.

[54] R. Di-Maio, C. De Paola, G. Forte et al., "An integrated geological, geotechnical and geophysical approach to identify predisposing factors for flowslide occurrence," *Engineering Geology*, vol. 267, article 105473, 2020.

[55] P. R. Pujari and A. K. Soni, "Sea water intrusion studies near Kovaya limestone mine, Saurashtra coast, India," *Environmental Monitoring and Assessment*, vol. 154, no. 1-4, pp. 93–109, 2009.